Cancer Research

Dual Functional Monoclonal Antibody PF-04605412 Targets Integrin α5β1 and Elicits Potent Antibody-Dependent Cellular Cytotoxicity

Gang Li[1], Lianglin Zhang[1], Enhong Chen[1], Jianying Wang[1], Xin Jiang[1], Jeffrey H. Chen[1], Grant Wickman[1], Karin Amundson[1], Simon Bergqvist[1], James Zobel[2], Dana Buckman[1], Sangita M. Baxi[1], Steven L. Bender[1], Gerald F. Casperson[2], and Dana D. Hu-Lowe[1]

Abstract

Integrin α5β1 is overexpressed in tumor-associated stroma and cancer cells, and has been implicated in angiogenesis, tumor survival, and metastasis. Antibody-dependent cellular cytotoxicity (ADCC) by immune effector cells has been shown to contribute to clinical efficacy for several IgG1 monoclonal antibody (mAb) therapeutics. Taking advantage of these two mechanisms, we generated a fully human, fragment crystalizable (Fc)-engineered IgG1 mAb, PF-04605412 (PF-5412), which specifically neutralizes α5 and binds the Fcγ receptors (FcγR) with enhanced affinity. *In vitro*, PF-5412 potently inhibited α5β1-mediated intracellular signaling, cell adhesion, migration, and endothelial cell (EC) tubulogenesis. PF-5412 induced significantly greater ADCC in α5-expressing tumor cells and ECs compared with a wild-type IgG1 (IgG1/wt) or IgG2 of identical antigen specificity. The degree of ADCC correlated with the abundance of natural killer (NK) cells in the peripheral blood mononuclear cells but was independent of donor FcγRIIIa polymorphism. In animal studies, PF-5412 displayed robust and dose-dependent antitumor efficacy superior to that observed with IgG1/wt, IgG2, or IgG4 of identical antigen specificity. The degree of efficacy correlated with α5 expression, macrophage and NK cell infiltration, and NK activity in the tumor. Depletion of host macrophages abrogated antitumor activity, suggesting a critical contribution of macrophage-mediated antitumor activity of PF-5412. Combination of PF-5412 with sunitinib significantly improved antitumor efficacy compared with either agent alone. The dual mechanism of action and robust antitumor efficacy of PF-5412 support its clinical development for the treatment of a broad spectrum of human malignancies. *Cancer Res; 70(24); 10243–54. ©2010 AACR.*

Introduction

Integrin α5β1 is a classic fibronectin (Fn) receptor that plays important roles in vascular biology including embryonic vasculogenesis, vascular remodeling, pathologic angiogenesis, and inflammation (1–3). Its involvement in the function of tumor-associated endothelium and stroma cells has also been reported (4). In response to proangiogenic factors, α5β1 promotes endothelial cell (EC) adhesion, migration, proliferation, survival, and differentiation (5, 6).

α5β1 is frequently overexpressed in tumor cells and has been associated with hypoxia, survival, epithelial-mesenchymal transition, invasion, and metastasis (7–9). Various studies have linked α5β1 upregulation with the progression of several cancers (10–13). The overall survival in patients with lung cancers and breast cancers was found to be inversely correlated with the degree of tumor α5 expression (8, 14), providing a basis for targeting α5β1 for cancer therapy. Among the several inhibitors against α5 is volociximab (M200; ref. 15). In the clinic, M200 generated disease stabilization and a number of partial responses in previously heavily treated metastatic renal cell carcinoma patients (16).

Accumulating evidence suggests that antibody-dependent cellular cytotoxicity (ADCC) may play a significant role in anticancer therapy (17). ADCC is a major immune effector mechanism in which target cell–bound antibody–antigen complexes engage innate immune effector cells via fragment crystalizable γ receptors (FcγR), resulting in the killing of antigen-expressing target cells (18–21). Clinical proof of principle for ADCC was shown for rituximab in non-Hodgkin lymphoma patients and trastuzumab in breast cancer

Authors' Affiliations: [1]Oncology Research Unit, Pfizer Inc., San Diego, California; and [2]Biotherapeutics Pharmaceutical Sciences, Pfizer Inc., St. Louis, Missouri

Note: Supplementary data for this article are available at Cancer Research Online (http://cancerres.aacrjournals.org/).

Current addresses for Xin Jiang: Sova Pharmaceuticals, La Jolla, CA; Grant Wickman: The Beatson Institute for Cancer Research, Glasgow, UK; and Karin Amundson: Tocagen Inc., San Diego, CA.

Corresponding Author: Dana D. Hu-Lowe, The Oncology Research Unit, Pfizer Inc., 10646 Science Center Drive, San Diego, CA 92121. Phone: 858-622-6019; Fax: 858-622-599. E-mail: dana.hu-lowe@pfizer.com

doi: 10.1158/0008-5472.CAN-10-1996

patients; in both cases, better therapeutic outcomes were associated with high-affinity allele of FcγRs, FcγRIIIa/158V, or FcγRIIa/131H (22–25). Additionally, in metastatic colorectal cancer patients treated with cetuximab, the ones harboring the high-affinity FcγRIIIa/158V allele survived significantly longer than those with 158F/F (26). Importantly, this correlation was independent of mutant K-ras status, underlining a significant contribution of ADCC to the clinical benefit from cetuximab.

Several technologies have been developed to improve the binding affinity between the Fc region and the FcγRs on effector cells (27, 28). Products through glycoengineering, GA101 (anti-CD20), GA201 (anti-EGFR), and MDX-1401 (anti-CD30) have shown increased ADCC and superior *in vivo* antitumor activity in preclinical models compared with rituximab, cetuximab, and MDX-060, respectively (29–31). XmAb5574, a humanized anti-CD19 IgG1 monclonal antibody (mAb) with enhanced ADCC via Fc mutagenesis, has entered clinical development as a potential therapy for B-cell malignancies (32).

We developed a fully human, ADCC-enhanced anti-α5 IgG1 mAb PF-5412 via amino acid mutations in the Fc region (33). In this report, we provide evidence of its robust *in vitro* and *in vivo* activities through ADCC and antibody-dependent phagocytosis (ADPC).

Materials and Methods

Antibodies and compounds

The following mAbs were made at Pfizer: PF-5412 (an IgG1 with DLE mutations in the Fc region), wild-type (wt) mAbs with identical variable domains but different constant regions (α5-IgG1/wt, α5-IgG2, and α5-IgG4), negative control antibodies keyhole limpet hemocyanin (KLH)-IgG1 and KLH-IgG1/DLE, and M200. Also generated at Pfizer are the following compounds: sunitinib [ref.34; a multi-targeted inhibitor of vascular endothelial growth factor receptors (VEGFR), platelet-derived growth factor receptors, Kit and Flt3], axitinib (35), and PF-0337210 (ref. 36; both are potent and selective small molecule inhibitors of VEGFRs). Bevacizumab (anti-VEGF mAb by Genentech) was purchased from Northeast Medical Products, Inc. All antibodies were dosed subcutaneously once a week (QW) at the indicated doses. Sunitinib and PF-0337210 were given orally once daily (QD), and axitinib was given orally twice daily (BID).

Cells

Human umbilical vein endothelial cells (HUVEC) and normal human dermal fibroblasts (NHDF) were purchased from Lonza. U87MG and A549 were obtained from American Type Culture Collection. M24met was described elsewhere (37). A549-luc-C8 was purchased from Xenogen. Other luciferase-expressing cells were made by transfection with vector pLPCX: Luc-SH. To overexpress α5, parental MV522 cells were infected with retroviral particles made in 293T cells with vector pBabe-puro/α5. Human or monkey peripheral blood mononuclear cells (PBMC) were isolated and maintained as described previously (38). FcγRIIIa polymorphism genotyping and natural killer (NK)% measurements by flow cytometry were performed according to published protocols (39). The generation of mouse, rabbit, and monkey α5-transfected cells is described in Supplementary Materials.

Generation of fully human anti-α5 hybridoma and antibodies from transgenic mice

Human transchromosomal/transgenic KM mice from Medarex, Inc. were immunized with 1×10^7 NIH3T3 cells overexpressing human α5. Sera from the immunized mice were screened by flow cytometry for binding to α5 in α5/NIH3T3 cells and to the parental NIH3T3 cells. Hybridomas were generated according to the standard procedure (40). Hybridomas expressing antibodies that bound α5/NIH3T3 cells, but not the parental cells, were cloned twice by limiting dilution.

Integrin α5β1 and FcγR binding assays and affinity determination

Antibody affinity for integrin α5β1 was measured by fluorescence-activated cell sorting (FACS) analysis and surface plasmon resonance (SPR) using a Biacore 3000 (GE Healthcare; see Supplementary Methods for details). Human FcγRI was purchased from R&D Systems. The other human and murine FcγRs were produced by transient expression in HEK293 cells, and purified using HisTrap FF columns (GE Healthcare). PF-5412 was immobilized on a CM5 sensor chip using the standard primary amine coupling protocol. FcγRs were infused followed by a 2- to 3-minute dissociation phase. Data were fit to a 1:1 binding model (Langmuir) using Scrubber2 data analysis software (BioLogic software). Kinetic variables were used to calculate the equilibrium dissociation constant (K_D).

In vitro ADCC assay

A total of 1×10^4 target cells were preincubated with mAbs at indicated concentrations. Human or monkey PBMCs were added at effector:target (E:T) cell ratio of 50∼100:1. Assay plates were incubated at 37°C for 4 hours. Cytolysis was determined using either the LDH Cytotoxicity Detection Kit (Roche) or the ToxiLight BioAssay Kit (Cambrex).

In vitro ADPC assay

Human donor monocytes were isolated using CD14 magnetic beads (Miltenyi Biotech) and differentiated into macrophages with 10 ng/mL granulocyte macrophage colony stimulating factor (R&D Systems) for 5 days. Macrophages and U87MG target cells were labeled with PKH26 (Sigma) and CMFDA (Invitrogen), respectively. Labeled U87MG cells were incubated with mAbs for 30 minutes and then added to the labeled macrophages. Four hours later, phagocytosis was determined by counting double-labeled cells by FACS analysis.

In vivo angiogenesis models

To establish the high-density (HD) Matrigel-based human angiogenesis model, a mixture of HUVEC (3×10^6) and NHDF cells (1×10^6) in HD Matrigel (BD Biosciences, 10 mg/mL) was implanted subcutaneously (0.8 mL/injection) in the flank of mice. After 4 to 6 weeks, the Matrigel plugs were removed and fixed in 1% paraformaldehyde at 4°C overnight, embedded in

ornithine carbamyl transferase, and sectioned for histology analysis.

Another model is the human foreskin–severe combined immunodeficient (SCID) mouse chimera based on the report by Tahtis and colleagues (41). Briefly, a piece of 1 cm × 2 cm human neonatal foreskin was sutured to the back of a BALB/c SCID mouse. After recovery (5–7 weeks), M24met cells (2×10^6) were intradermally injected into the engrafted human skin. When tumor volume reached between 50 and 100 mm^3, the mice were randomized to receive treatments. Human-specific CD31 staining was then used to detect human vessels (42).

Human PBMC/U87MG-luc immunoxenograft model

A 100-μL mixture of human PBMCs (0.5×10^6) and U87MG-luc (1×10^6) in 100 μL of Matrigel (BD Biosciences) was subcutaneously injected to mice. Tumor growth was monitored by bioluminescence imaging (BLI) and/or digital caliper measurements.

Experimental metastasis model

A549-luc-C8 cells (3×10^6/100 μL) were injected intravenously into BALB/c SCID mice that had received a single predose 2 days prior. The animals were treated with indicated antibodies for 8 weeks. BLI was carried out once a week until the end of the study.

In situ macrophage depletion in mice

Clodronate-liposomes (5.5 mg/mL) or PBS-liposomes (25–200 nm in mean particle diameters) were purchased from Dr. Nico van Rooijen's laboratory (Vrije University, Amsterdam, the Netherlands). One day before tumor implant, 2 injections of the liposome particles were given to mice (2.5 mg/g body weight, intravenously and 50 μL, subcutaneously, near the site of tumor implantation). The particles were subsequently given intravenously twice a week until end of the study.

Immunohistochemistry staining and quantification of NK cells and macrophages

Murine NK cells were stained with antimouse NK1.1 (Biolegend), and macrophages were stained using a rat antimouse antibody for macrophage marker F4/80 (Abcam; ref. 43). Tissue immunohistochemistry (IHC) images were captured using an Olympus MicroFire digital camera and PictureFrame software. Percentage of positive staining was quantified using the ChromaVision Automated Cell Imaging System.

Statistical analysis

Statistical significance was determined by analysis of variance using Dunnett's multiple-comparison post-test with GraphPad Prism software unless otherwise noted.

Results

Generation of PF-5412

The mAb PF-5412 was derived from α5-IgG1/wt by mutagenesis in the Fc region to introduce 3 mutations, S239D/A330L/I322E (DLE), that have been reported to enhance ADCC activity (33), and by mutagenesis of the variable domains to return several framework residues to those encoded in the germ line (for details see Supplementary Methods).

In vitro antigen binding and neutralization activities of PF-5412

SPR- and FACS-based assays showed that PF-5412 bound to human α5β1 with nanomolar affinity (Table 1; Fig. 1A). The K_D values (2.7 nmol/L for PF-5412 and 2.2 nmol/L for α5-IgG1/wt) indicated that Fc engineering did not alter antigen binding affinity. Competition binding experiments using SPR indicated that PF-5412 and M200 bound at the same binding site on α5β1 (Supplementary Fig. S1A and B). In cellular assays, PF-5412 blocked HUVEC cell adhesion to Fn with a similar potency as α5-IgG1/wt, α5-IgG2, and M200 (Fig. 1B). In addition, PF-5412 dose dependently blocked HUVEC migration (Supplementary Fig. S1C). In a coculture tubule formation assay, PF-5412 exhibited a dose-dependent activity similar to axitinib (Fig. 1C). PF-5412 also inhibited total and phosphorylated focal adhesion kinase (FAK; Fig. 1D), a downstream signaling molecule of α5β1. Consistent with α5β1's role in EC survival, PF-5412 induced caspase 3/7–mediated apoptosis of HUVEC with an EC_{50} value of 15.3 nmol/L (Supplementary Fig. S1D). PF-5412 was found to bind to integrin α5 of cynomolgus monkey and rabbit, but not to that of rat or mouse (Table 1). Consistent with its binding affinity to cynomolgus α5, PF-5412 inhibited monkey monocyte adhesion to Fn in an *ex vivo* assay (Supplementary Fig. S1E). These data are summarized in Table 1.

In vitro FcγR binding and ADCC/ADPC activity

Compared with α5-IgG1/wt, PF-5412 showed enhanced affinity for FcγRI, FcγRIIIa, and other FcγRs ranging from 6-fold to 122-fold as assessed by the SPR assay. In addition, PF-5412 showed enhanced affinity for all 3 murine FcγRs tested (Table 1; Supplementary Fig. S2A).

In *in vitro* ADCC assays using U87MG (target cells) and human PBMCs, PF-5412 induced a 40% ADCC (EC_{50} = 0.04 nmol/L), whereas α5-IgG1/wt induced a 15% ADCC (EC_{50} = 0.13 nmol/L; Fig. 2A, left). A similar result was observed when HUVECs were used as target cells (Fig. 2A, right). In the same assays, α5-IgG4, α5-IgG2, or M200, all of which have minimal intrinsic ADCC capability, did not induce measurable cytolysis. An enhanced ADCC was also observed with monkey PBMCs and U87MG cells (Supplementary Fig. S2B). The maximum degree of ADCC ($ADCC_{max}$) observed with a given human donor's PBMCs positively correlated with α5β1 receptor density on the various target cells (Fig. 2B, i; Supplementary Fig. S2C). Importantly, PF-5412, but not α5-IgG1/wt, was able to induce significant ADCC in cell lines that expressed a wide range of α5 (Fig. 2B, ii–iv).

When fully differentiated human macrophages were mixed with U87MG cells, phagocytosis was observed in the presence of PF-5412 and α5-IgG1/wt (0.1 μg/mL and 1 μg/mL), but not the KLH control mAbs. At either concentration, PF-5412 induced a greater degree of phagocytosis than α5-IgG1/wt (Fig. 2C). These data indicate that PF-5412 has a greater potential to kill target cells through ADPC than α5-IgG1/wt.

Table 1. Key *in vitro* attributes of PF-5412

Assay and parameter	Method	Value (nmol/L, unless otherwise noted)
Affinity for α5β1	SPR	
K_D		5.5 ± 0.3
On rate [k_{on}, $(mol/L)^{-1}s^{-1}$]		2.0 ± 0.05 × 10^5
Off rate (k_{off}, s^{-1})		1.1 ± 0.05 × 10^{-3}
Bivalent avidity (K_D) for α5β1	SPR	0.05
Binding (K_D) to cellular human α5β1	FACS	
Jurkat cells		0.79
HUVECs		2.15
Binding (K_D) to cellular monkey α5β1	FACS	
Monkey α5/NIH3T3		2.0
Binding (K_D) to cellular rabbit α5β1	FACS	
Rabbit α5/NIH3T3		2.9
Binding to cellular rat and mouse α5β1	FACS	No binding up to 660 nmol/L
Biacore (K_D) binding to FcγRs (Fold enhancement over α5-IgG1/wt)	SPR	
Human FcγRI		5.8 (6×)
Human FcγRIIa/131H		1,000 (1.6×)
Human FcγRIIa/131R		650 (2.3×)
Human FcγRIII/158F		27 (122×)
Human FcγRIII/158V		9.4 (70×)
Murine FcγRI		96 (14×)
Murine FcγRIII		1,700 (5×)
Murine FcγRIV		9.1 (260×)
HUVEC adhesion to fibronectin (EC_{50})	Adhesion assay	1.0
Inhibition of intracellular signal transduction	Western blotting	
Total FAK and phospho-FAK modulation		YES
Inhibition of HUVEC migration	Transwell assay	YES
Induction of HUVEC apoptosis (EC_{50})	Caspase-Glo 3/7	15.3
In vitro ADCC activity (EC_{50}, range of cytolysis)	LDH release or Toxilight assays	
Human PBMCs:HUVECs		0.098 (40%–80%)
Human PBMCs:U87MG cells		0.04 (40%–80%)
Monkey PBMCs:U87MG cells		0.03 (up to 70%)
In vitro phagocytosis (ADPC) activity	FACS	
Human macrophages:U87MG cells		YES

To investigate if ADCC was influenced by FcγRIIIa polymorphism, ADCC assays were performed with PBMCs from 14 donors representing all 3 FcγRIIIa genotypes. There was no correlation between $ADCC_{max}$ and FcγRIIIa polymorphism (Fig. 2D, left). However $ADCC_{max}$ positively correlated with the percentage of NK cells in PBMCs (Fig. 2D, right), indicating that NK cells played an important role in target cell cytolysis.

In vivo antiangiogenesis activity

Because PF-5412 does not cross-react with rodent α5β1, *in vivo* angiogenesis models containing human ECs were established. In the HD Matrigel-based human angiogenesis model, PF-5412 reduced human $CD31^+$ vessels compared with vehicle or the isotype-matched KLH mAbs, α5-IgG1/wt and bevacizumab (Fig. 3A; $^*P < 0.05$ in Supplementary Fig. S3A). In a separate study, PF-5412 was more effective than M200 at 3 mg/kg, and the 2 agents showed similar antiangiogenic activity at 10 mg/kg (Supplementary Fig. S3B).

In the human foreskin–SCID mouse chimera model in which human vessels were present and expressed human α5 (44), single injections of PF-5412 dose dependently inhibited human $CD31^+$ vessel formation (Fig. 3B) with an *in vivo* ED_{50} of 1.2 mg/kg and ED_{90} of 4.6 mg/kg (Fig. 3B, inset).

Antitumor efficacy

In CB17.SCID mice with functional NK cells and macrophages, weekly administration of PF-5412 at either 1 mg/kg or 10 mg/kg significantly delayed the growth of the U87MG tumors (Fig. 3C, left). The degree of tumor growth inhibition (TGI) by the high dose of PF-5412 (86%) was greater than that by bevacizumab (69%). Antitumor efficacy of PF-5412, but not

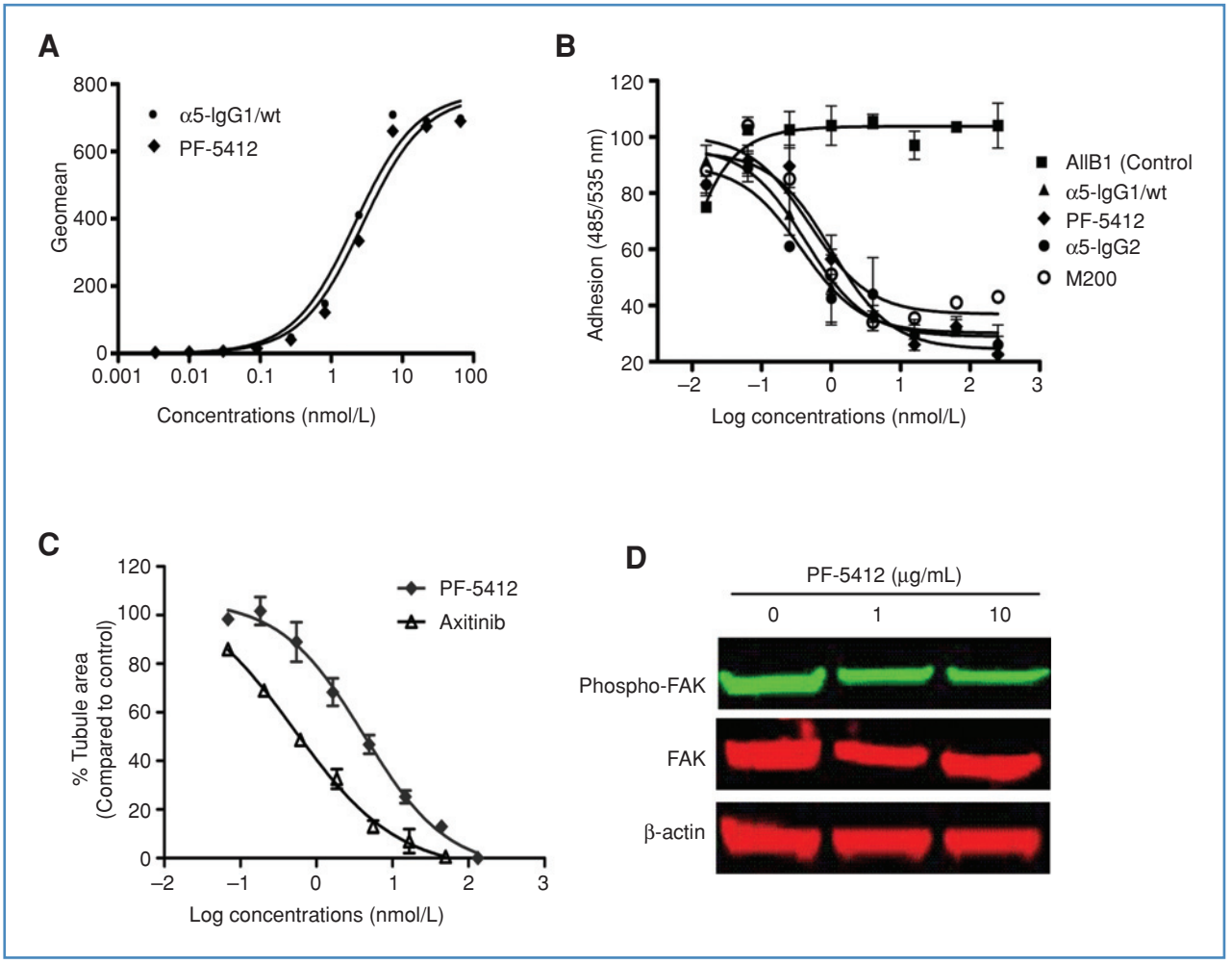

Figure 1. *In vitro* potency and activity of PF-5412. A, dose-dependent binding of PF-5412 and α5-IgG1/wt to HUVEC measured by FACS. B, dose-dependent inhibition of HUVECs adhesion to Fn by anti-α5 mAbs. Similar potency was observed for PF-5412 compared with α5-IgG1/wt, α5-IgG2, and M200. C, dose-dependent inhibition of tubule formation in a human ECs/fibroblast cell coculture assay. Axitinib is a VEGF receptor tyrosine kinase inhibitor used as a positive control. D, inhibition of both total and phospho-FAK in U87MG cells by PF-5412 in a Western blotting assay.

bevacizumab, was associated with increased tumor infiltration of NK cells and macrophages (Fig. 3C, right).

We next assessed the TGI of PF-5412 in an immunoxenograft model in which U87MG-luc cells and human PBMCs were coimplanted in CB17.SCID/beige mice (deficient in host NK). In this model, the human PBMCs served as a source of neutrophils and NK cells, whereas the mouse supplied macrophages. PF-5412 treatment induced tumor regression at 3 and 10 mg/kg. M200 generated moderate TGI (40%; Fig. 3D, left; Supplementary Fig. S3C). Compared with α5-IgG1/wt and M200, PF-5412–treated tumors showed increased NK cell activity (Granzyme B), a greater number of macrophages, and a higher degree of tumor cell apoptosis (Fig. 3D, right; Supplementary Fig. S3D). A separate study showed that the extent of antitumor efficacy correlated with the number of human PBMCs coimplanted with the tumor cells (not shown). These results indicated that human NK cells and potentially host macrophages contributed significantly to antitumor efficacy of PF-5412.

Host macrophages contribute significantly to efficacy

We then used tumor-bearing CB17.SCID/beige mice (NK deficient) to address whether host macrophages alone could play a significant role in the activity of PF-5412. We observed that PF-5412, but not M200, significantly and dose dependently inhibited U87MG-luc tumor growth (Fig. 4A); the TGI was associated with a dose-dependent increase in mouse macrophage infiltration in the tumor (Fig. 4B). When the host macrophages were depleted by clodronate-liposomes (45), the TGI was significantly compromised compared with mice treated with PBS-liposomes (Fig. 4C; Supplementary Fig. S4A). The effect was not because of any intrinsic activity of clodronate as clodronate-liposomes alone did not affect tumor growth (Fig. 4C). These data strongly suggest that the efficacy of PF-5412 is dependent on ADPC from mouse macrophages.

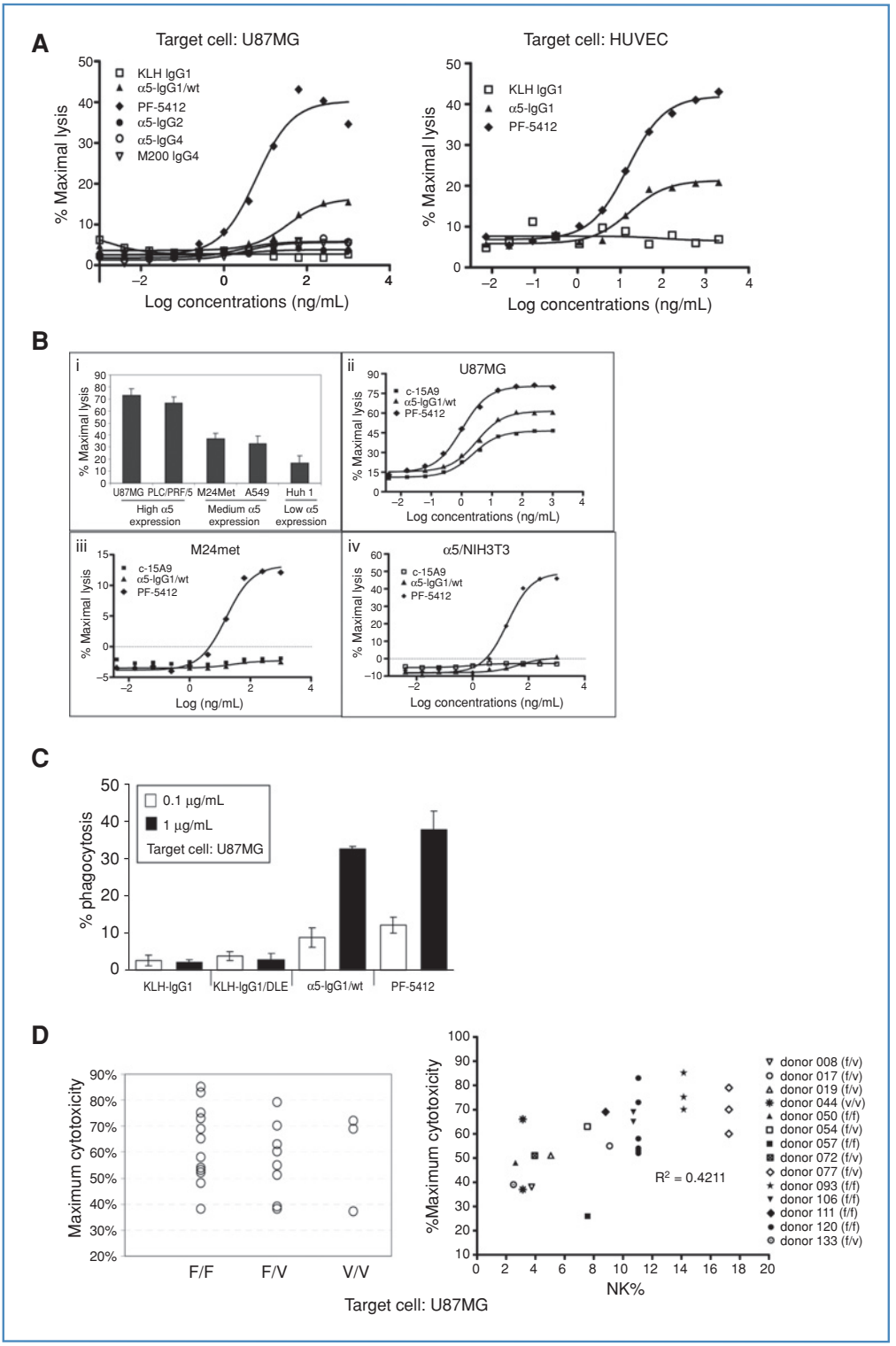

Figure 2. *In vitro* ADCC and ADPC assessments. A, dose-dependent cytolysis (ADCC) of U87MG cells (left) and HUVEC (right) in the presence of PBMCs from a human donor and anti-α5 antibodies including PF-5412. In U87MG cells, the EC_{50} of PF-5412 is 0.04 nmol/L, and in HUVEC, the EC_{50} of PF-5412 is 0.098 nmol/L. B, i, PF-5412 induced ADCC of several target cell lines expressing varying levels of α5. The relative α5 expression levels are indicated underneath the bars. ii–iv, dose-dependent ADCC by PF-5412 compared with α5-IgG1/wt in 3 target cell lines expressing varying amount of α5. C, PF-5412 induced ADPC of U87MG cells in the presence of human macrophages as measured by FACS. PF-5412 produced a greater degree of ADPC compared with α5-IgG1/wt although the difference did not reach statistical significance. D, correlation analysis of maximal U87MG cytolysis by PF-5412 with FcγRIIIa polymorphism (left) and NK% in PBMCs (right) from 14 healthy donors.

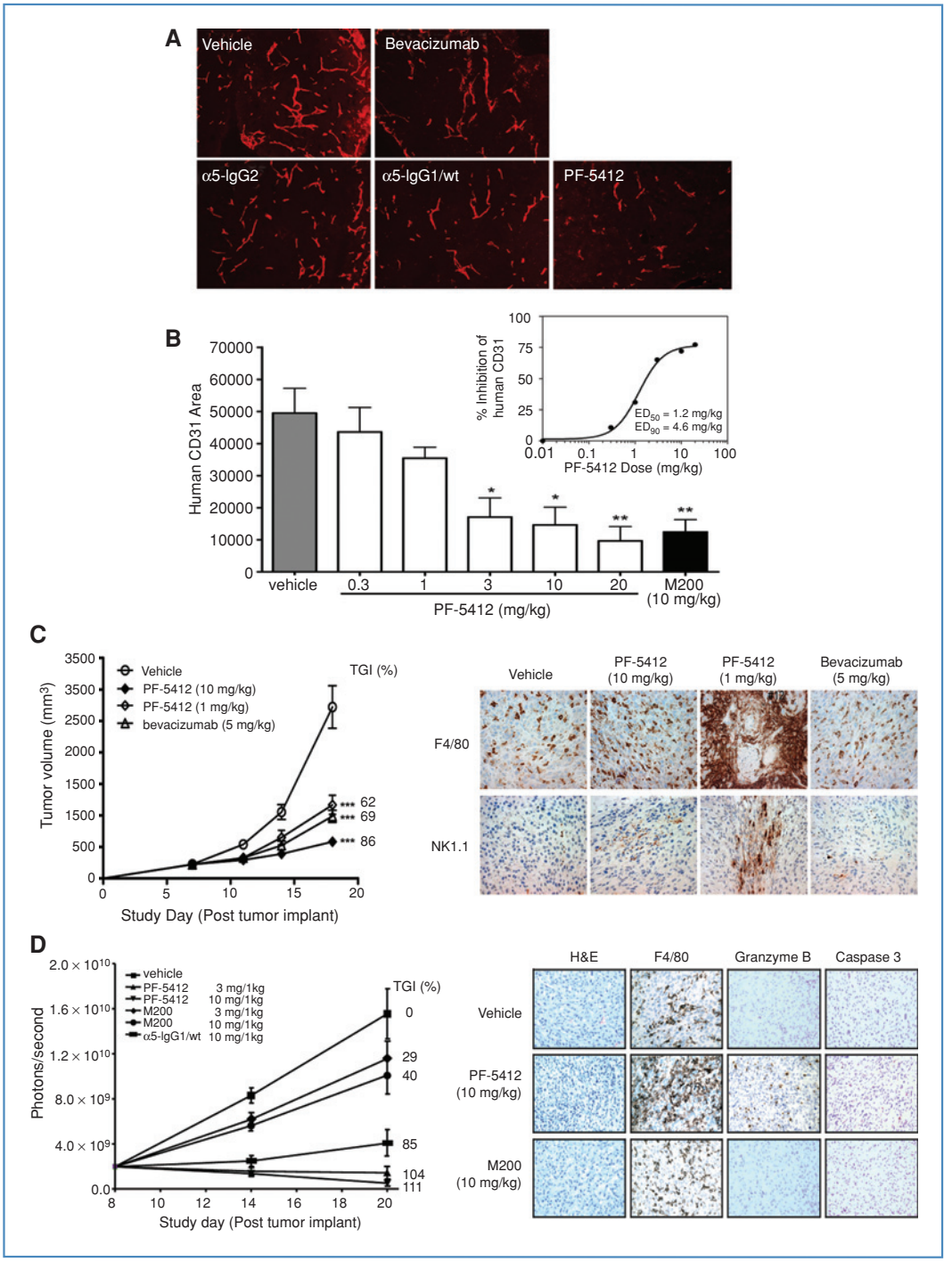

Figure 3. Characterization of PF-5412 for its antiangiogenesis and antitumor efficacy. A, inhibition of human blood vessel growth in the HD Matrigel-based human angiogenesis model by PF-5412 and α5-IgG2 or IgG1/wt. Shown are representative fluorescent images (10X) of human CD31 staining (red). Bevacizumab was used as a positive control. B, dose-dependent antihuman angiogenesis effect of PF-5412 in the human foreskin–SCID mouse chimera model. Tumors were resected at the end of a single-dose 7-day treatment and human CD31 was stained and quantified. M200 was also tested in this study. *, $P < 0.05$; **, $P < 0.01$. Inset shows the derivation of ED_{50} and ED_{90} when the dose-response values were fitted to a sigmoid curve. C, antitumor efficacy of PF-5412 in U87MG subcutaneous xenograft tumor model and associated effector cell infiltration. Treatments began on day 7 when the average tumor size was about 200 mm^3. Left, growth delay curves; tumor volume was presented as group mean ± SEM. ***, $P < 0.001$ compared with the vehicle group. Bevacizumab was used as a comparator. $n = 10$/group. Right, representative images of infiltrated macrophages (F4/80, brown) and NK cells (NK1.1, brown) in tumors. Magnification, ×40. D, left, Bioluminescence measurements of the growth of U87MG-luc mixed with human PBMCs in CB17.SCID/beige mice under treatment of PF-5412, α5-IgG1/wt, or M200. Weekly treatments began on day 8. Right, Representative photographs of hematoxylin and eosin and IHC staining for F4/80, granzyme B (brown), and activated caspase-3 (brown) in tumors harvested 4 days after a single dose of either PF-5412 or M200. $n = 8$ per group. Magnification, ×40.

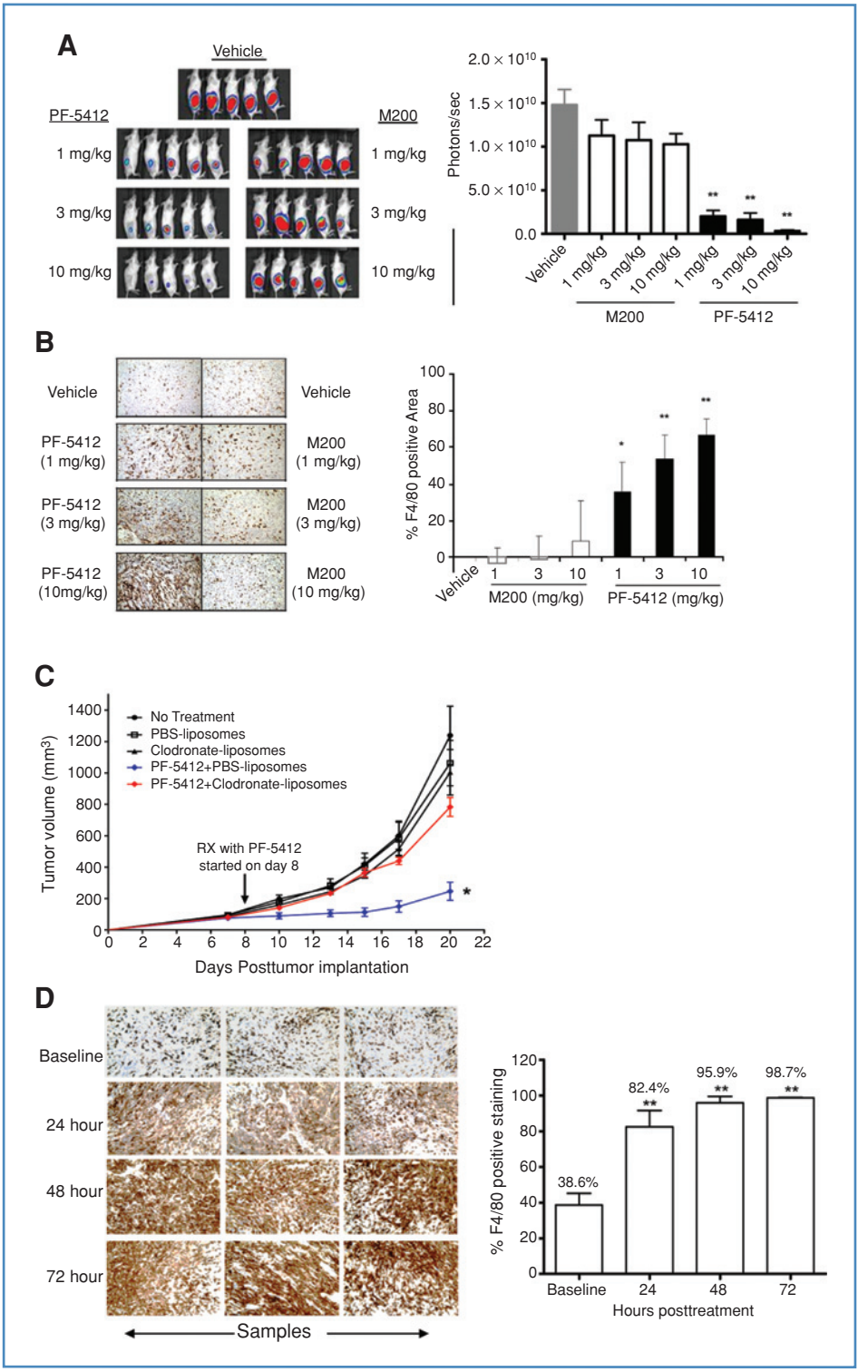

Figure 4. Elucidating contribution of macrophage in U87MG-luc xenografts implanted CB17.SCID/beige mice. A, antitumor activity of PF-5412 or M200. Shown are representative BLI images (left) and BLI quantitation of tumor cells (right) 20 days postdose. Data are shown as group mean ± SEM, $n =$ 10 per group. **, $P < 0.01$ for PF-5412 at all doses compared with vehicle or M200. B, dose-dependent macrophage infiltration in the U87MG tumors after a 3-week treatment by either PF-5412 or M200. Left, representative images of tumors stained with anti-F4/80 (brown, ×20); Right, area of F4/80 staining was quantified using automated cell imaging system (Chromvision). *, $P < 0.05$ and **, $P < 0.01$, compared with vehicle; Bars, group mean ± SEM; $n = 10$ per group. C, depletion of host macrophages with clodronate-liposomes diminished antitumor efficacy of PF-5412 in the CB17.SCID/beige mice bearing U87MG tumor. *, $P < 0.05$ versus PF-5412 + clodronate-liposomes. Error bars, SEM; $n =$ 10 per group. D, rapid tumor macrophage infiltration following PF-5412 administration. Tumor samples were collected at indicated time points after a single dose of PF-5412 (10 mg/kg). Left, 3 representative images of F4/80 positive (brown) tumor tissue sections for each time point. Right, quantification of F4/80 intensity. Bars, group mean ± SD ($n = 5$ per group). **, $P < 0.01$ compared with baseline prior to treatments.

The influx of macrophages was detectable 24 hours after a single dose of PF-5412 (10 mg/kg) and continued to increase through 72 hours postdose (Fig. 4D). In a separate study, elevated levels of macrophages in the tumor were observed for as long as 7 days following a single dose of PF-5412 (data not shown). A single dose of PF-5412 also induced a marked reduction of phosphorylated FAK and total FAK in the tumor (Supplementary Fig. S4B), suggesting a direct effect on α5β1 signaling in addition to or as a consequence of ADCC and ADPC by PF-5412.

Macrophage-mediated ADPC and efficacy requires the presence of α5

PF-5412 produced a greater TGI with MV522/α5 tumors engineered to express a moderate level of α5 (clone 11), compared with clone 1 that expressed a lower level of α5 (Supplementary Fig. S5A), or the parental cells (do not have detectable a5; Fig. 5A). The TGI was associated with increased intratumoral macrophage staining in MV522/α5 clone 11, but not clone 1 (Fig. 5B).

Antimetastatic activity of PF-5412

In the lung metastasis model of A549-Luc-C8, an 8-week treatment with PF-5412 and α5-IgG2 exhibited significant antimetastatic efficacy with a TGI of 97% and 89% (week 8), respectively (Fig. 5C, left). After dosing was stopped, tumors in the PF-5412–treated group remained suppressed through week 13, whereas those in α5-IgG2–treated group began to regrow 2 weeks after dosing cessation. PF-5412 significantly extended the median time-to-progression to 20 weeks or more compared with 14 weeks and 10 weeks for α5-IgG2 and the vehicle group, respectively (Fig. 5C, right).

Combination of low-dose PF-5412 with sunitinib or bevacizumab significantly enhanced antitumor efficacy

We further assessed efficacy of combination of low-dose PF-5412 with sunitinib, an agent with a different antiangiogenic mechanism of action than PF-5412. In the U87MG-luc tumor model in CB17.SCID/beige mice, PF-5412 (1 mg/kg) and sunitinib (30 mg/kg, a suboptimal dose) produced TGI of 46% and 32%, respectively; the combination treatment produced an 83% TGI, significantly better than either monotherapy alone ($P < 0.05$ versus PF-5412 and $P < 0.001$ versus sunitinib; Fig. 5D; Supplementary Fig. S5B). In the same study, M200 (1 mg/kg) alone generated a 26% TGI, which was improved to 41% when combined with sunitinib. This latter TGI was significantly less ($P < 0.01$) compared with that of PF-5412 in combination with sunitinib (Supplementary Fig. S5B).

Discussion

In this report, we showed that PF-5412, a fully human dual functional mAb against integrin α5β1, potently and dose dependently blocked EC adhesion, migration, tubule formation, and survival (Fig. 1). The mAb also inhibited angiogenesis mediated by human endothelial cells/vessels in *in vivo* models developed to harbor the human angiogenesis components (Fig. 3A and B). More importantly, as a result of Fc engineering to improve binding affinities to FcγRs, PF-5412 elicited enhanced ADCC/ADPC activity through host immune effector cells resulting in superior target cell lysis (Fig. 2A and C), robust antitumor and antimetastasis activities in a cohort of xenograft tumor models compared with α5-IgG1/wt, α5-IgG2, α5-IgG4, and M200 mAbs (Figs. 3C and D, 4A, and 5C). These are consistent with reports for other antibodies carrying enhanced FcγR binding capacity (30, 31, 33, 46, 47). We further provided evidence on the molecular and cellular levels (Figs. 3C and D, 4B, and 5A; Supplementary Fig. S4A), and pharmacologic level (Figs. 3D and 4C) that NK-mediated ADCC and macrophage-mediated ADPC significantly and positively impacted efficacy of PF-5412. Importantly, we showed a rapid immobilization of macrophages in the tumor (as early as 24 hours postdose; Fig. 4D) prior to measurable TGI, suggesting an active role of macrophages in tumor elimination. In addition, we showed that ADCC/ADPC-mediated activity is dependent on the presence and density of the antigen (α5β1) expressed on target cells (Figs. 2B and 5A). To our knowledge this is the first report with comprehensive *in vitro* and *in vivo* characterization of an ADCC/ADPC-enhanced therapeutic antibody targeting solid tumors.

We observed that PF-5412 produced a similar $ADCC_{max}$ with donor PBMCs regardless of the allele variation of FcγRIIIa (Fig. 2D). Cancer patients with the low-affinity allele FcγRIIIa/158F have been associated with worse responses to rituximab (23, 24), trastuzumab (25), and cetuximab (26). In PF-5412, the binding affinities for the low-affinity FcγRIIIa/158F and FcγRIIa/131R were more significantly enhanced than for the higher affinity counterparts (Table 1; Supplementary Fig. S2A). As a result, the impact of allelic variations of the FcγRs on the degree of ADCC/ADPC was reduced. Similar observations were also reported for a low-fucose variant of rituximab (48). In addition, our *in vitro* data suggest that effector function enhancement in PF-5412 lowered the target density threshold required to produce cytolytic and antitumor efficacy compared with α5-IgG1/wt (Figs. 2A and B, 3D, 4A and B, and 5B and C). Given the prevalence of FcγRIIIa/158F allele (40% V/F and 40% F/F) in the general population (33) and the varying levels of α5β1 expression in patient tumors (unpublished observation), we believe that an ADCC/ADPC-enhanced mAb has the potential to impact a much larger and heterogeneous patient population in the clinic than would a wild-type mAb. It is also worth noting that although U87MG cells were used in many of the experiments, the potential indication of PF-5412 should not be limited to glioblastoma. In this study, the selection of the preclinical models for proof-of-principle studies was mainly based on the expression of the target in a model.

One of the strategies for rational combination is to simultaneously target multiple processes involved in cancer progression to provide meaningful benefit and circumvent resistance. Indeed, in the aggressive U87MG-luc mode, where single-agent sunitinib has not shown robust activity (unpublished data and ref. 49), combining a low dose of PF-5412 (1 mg/kg), but not M200, with a low dose of sunitinib (half of the projected clinically equivalent dose) produced a robust and

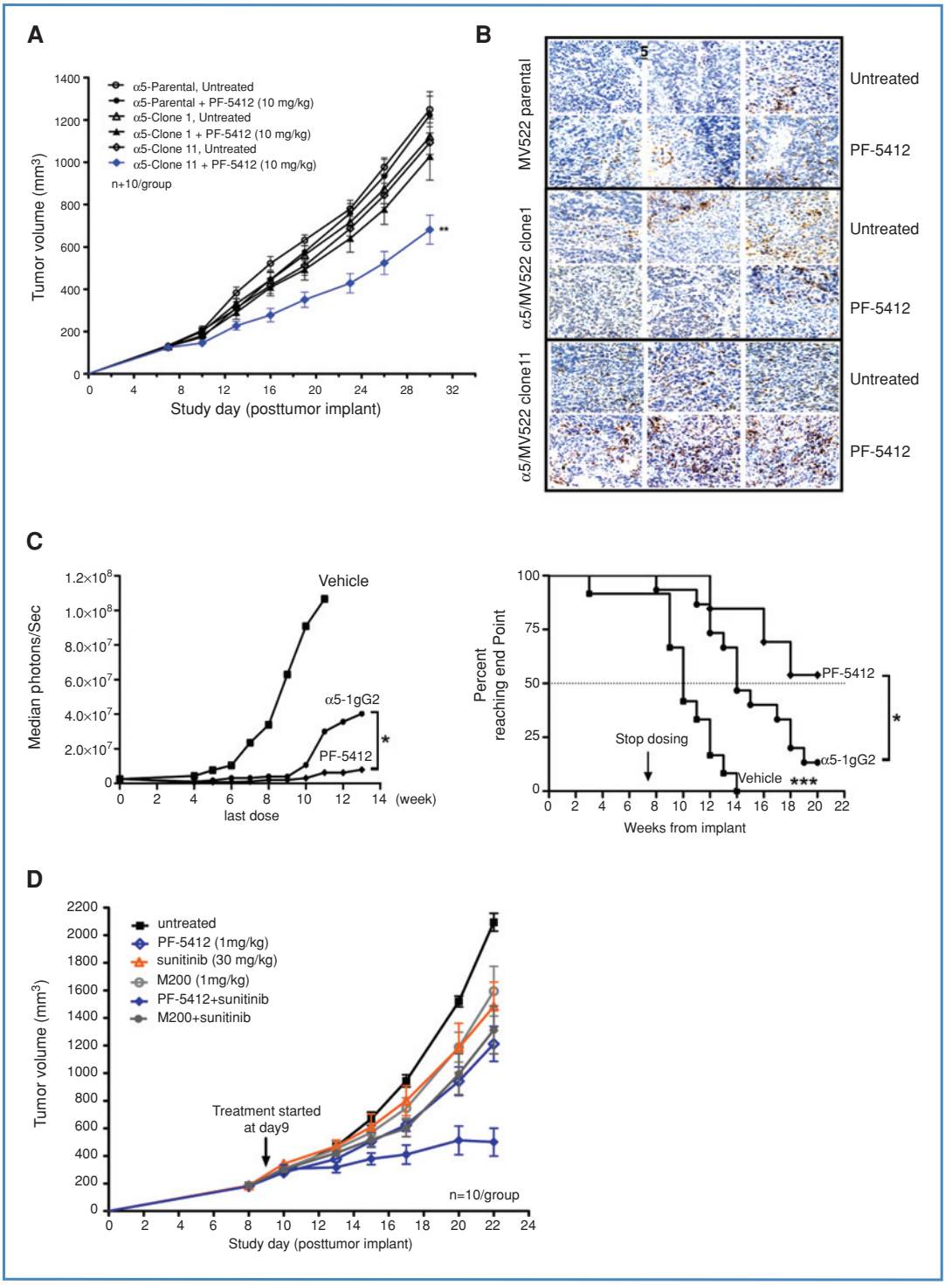

Figure 5. α5-Dependent antitumor, antimetastasis, and combination efficacy of PF-5412. A, antitumor efficacy of PF-5412 correlated with α5 expression. MV522 parental and α5 transfected clone 1 (low α5) and clone 11 (moderate α5) cells were implanted into CB17.SCID/beige mice and antitumor efficacy of PF-5412 was assessed. Treatments began on day 7. Tumor volumes are presented as group mean ± SEM ($n = 10$ per group). **, $P < 0.01$ compared with other groups. B, corresponding intratumoral macrophages (F4/80, brown) from each group at the end of the study. Increased F4/80 staining was observed in Clone 11 tumors treated with PF-5412 (bottom row). C, antimetastasis activity in A549-luc experimental metastasis model. Left, lung tumor burden of vehicle, PF-5412, and α5-IgG2 mAbs (both at 10 mg/kg, QW) was assessed by BLI. Treatment started 2 days before tail vein tumor injection and lasted for 8 weeks (arrow). *, $P = 0.037$ between PF-5412 and α5-IgG2 (week 13). Right, Kaplan–Meier plot of animal survival in each treatment group (end point $= 1 \times 10^8$ photons/second). ***, $P < 0.0001$ for vehicle compared with all other groups, and *, $P < 0.05$ between PF-5412 and α5-IgG2 groups. D, efficacy assessment of low-dose PF-5412 or M200 plus sunitinib (PO, QD) in the C.17 SCID/beige mice bearing U87MG-luc tumors. A synergistic effect was observed for PF-5412 + sunitinib but no efficacy enhancement for M200 + sunitinib. The table of statistics is presented in Supplementary Figure S5B.

greater than additive antitumor efficacy (tumor stasis; Fig. 5D). One possible explanation for the synergistic antitumor activity may be that sunitinib treatment induced tumor hypoxia, which in turn upregulated α5β1 (7) and sensitized α5β1-mediated tumor survival pathway. PF-5412 would be able to disrupt these events by blocking the augmented α5β1 signaling and eliciting strong ADCC/ADPC. Another hypothesis may include phagocytic macrophage subclass sequestration by PF-5412 to mitigate the recruitment and activation of bone marrow–derived immunosuppressive cells (including monocytes and proinflammatory macrophages) known to contribute to resistance to antiangiogenic therapies (50). Research is underway to gain further understanding of the observed synergism. In summary, our data imply that such a rational combination strategy may be a safe and robust approach for the treatment of aggressive tumors.

From a clinical development prospective, M200, an α5β1 neutralizing mAb, has shown that inhibiting integrin α5β1 in the clinic is safe and may provide incremental benefit to some cancer patients. Given the observations from this study, we believe that α5β1 neutralization may be necessary, but not sufficient, to produce a robust and sustained antitumor efficacy. Thus PF-5412 may represent a new-generation integrin-targeting modality that as a single agent or in combination may deliver a meaningful benefit to a broader cancer patient population in the clinic.

Disclosure of Potential Conflicts of Interest

G. Li, L. Zhang, E.H. Chen, J. Wang, J.H. Chen, S. Bergqvist, J. Zobel, D. Buckman, S.M. Baxi, S.L Bender, G.F. Casperson, and D.D. Hu-Lowe are full-time Pfizer employees. X. Jiang, G. Wickman, and K. Amundson are former Pfizer employees.

Acknowledgments

We thank Brett Simmons, David Kang, Taylor Buckley, Stephanie Hall, Shile Liang, Tina Lu, and Comparative Medicine for laboratory and husbandry support; Histopathology core of Pfizer La Jolla for support and expertise in sample processing and histologic analysis; Husam Younis, Eugenia Kraynov, Leslie Sharp, Levinia Lewis, and Leianna Bettencourt for project support; Jamie Christensen and Neil Gibson for guidance and discussion of the manuscript.

The costs of publication of this article were defrayed in part by the payment of page charges. This article must therefore be hereby marked *advertisement* in accordance with 18 U.S.C. Section 1734 solely to indicate this fact.

Received 06/03/2010; revised 09/30/2010; accepted 10/20/2010; published Online 12/15/2010.

References

1. Francis SE, Goh KL, Hodivala-Dilke K, Bader BL, Stark M, Davidson D, et al. Central roles of alpha5beta1 integrin and fibronectin in vascular development in mouse embryos and embryoid bodies. Arterioscler Thromb Vasc Biol 2002;22:927–33.
2. Muschler JL, Horwitz AF. Down-regulation of the chicken alpha 5 beta 1 integrin fibronectin receptor during development. Development 1991;113:327–37.
3. Serini G, Valdembri D, Bussolino F. Integrins and angiogenesis: a sticky business. Exp Cell Res 2006;312:651–8.
4. Magnussen A, Kasman IM, Norberg S, Baluk P, Murray R, McDonald DM. Rapid access of antibodies to alpha5beta1 integrin overexpressed on the luminal surface of tumor blood vessels. Cancer Res 2005;65:2712–21.
5. Collo G, Pepper MS. Endothelial cell integrin alpha5beta1 expression is modulated by cytokines and during migration in vitro. J Cell Sci 1999;112:569–78.
6. Takagi J, Strokovich K, Springer TA, Walz T. Structure of integrin alpha5beta1 in complex with fibronectin. EMBO J 2003;22:4607–15.
7. Mousa SA, Lorelli W, Campochiaro PA. Role of hypoxia and extracellular matrix-integrin binding in the modulation of angiogenic growth factors secretion by retinal pigmented epithelial cells. J Cell Biochem 1999;74:135–43.
8. Korah R, Boots M, Wieder R. Integrin alpha5beta1 promotes survival of growth-arrested breast cancer cells: an in vitro paradigm for breast cancer dormancy in bone marrow. Cancer Res 2004;64:4514–22.
9. Jin H, Varner J. Integrins: roles in cancer development and as treatment targets. Br J Cancer 2004;90:561–5.
10. Edward M. Integrins and other adhesion molecules involved in melanocytic tumor progression. Curr Opin Oncol 1995;7:185–91.
11. Sawada K, Mitra AK, Radjabi AR, Bhaskar V, Kistner EO, Tretiakova M, et al. Loss of E-cadherin promotes ovarian cancer metastasis via alpha 5-integrin, which is a therapeutic target. Cancer Res 2008;68:2329–39.
12. Shinohara M, Nakamura S, Sasaki M, Kurahara S, Ikebe T, Harada T, et al. Expression of integrins in squamous cell carcinoma of the oral cavity. Correlations with tumor invasion and metastasis. Am J Clin Pathol 1999;111:75–88.
13. Blase L, Daniel PT, Koretz K, Schwartz-Albiez R, Moller P. The capacity of human malignant B-lymphocytes to disseminate in SCID mice is correlated with functional expression of the fibronectin receptor alpha 5 beta 1 (CD49e/CD29). Int J Cancer 1995;60:860–6.
14. Adachi M, Taki T, Higashiyama M, Kohno N, Inufusa H, Miyake M. Significance of integrin alpha5 gene expression as a prognostic factor in node-negative non-small cell lung cancer. Clin Cancer Res 2000;6:96–101.
15. Bhaskar V, Fox M, Breinberg D, Wong MH, Wales PE, Rhodes S, et al. Volociximab, a chimeric integrin alpha5beta1 antibody, inhibits the growth of VX2 tumors in rabbits. Invest New Drugs 2008;26:7–12.
16. Kuwada SK. Drug evaluation: volociximab, an angiogenesis-inhibiting chimeric monoclonal antibody. Curr Opin Mol Ther 2007;9:92–8.
17. Griggs J, Zinkewich-Peotti K. The state of the art: immune-mediated mechanisms of monoclonal antibodies in cancer therapy. Br J Cancer 2009;101:1807–12.
18. Becknell B, Caligiuri MA. Natural killer cells in innate immunity and cancer. J Immunother 2008;31:685–92.
19. Yan L, Hsu K, Beckman RA. Antibody-based therapy for solid tumors. Cancer J 2008;14:178–83.
20. Wang SY, Weiner G. Complement and cellular cytotoxicity in antibody therapy of cancer. Expert Opin Biol Ther 2008;8:759–68.
21. Weiner GJ. Monoclonal antibody mechanisms of action in cancer. Immunol Res 2007;39:271–8.
22. Cartron G, Dacheux L, Salles G, Solal-Celigny P, Bardos P, Colombat P, et al. Therapeutic activity of humanized anti-CD20 monoclonal antibody and polymorphism in IgG Fc receptor FcgammaRIIIa gene. Blood 2002;99:754–8.
23. Weng WK, Levy R. Two immunoglobulin G fragment C receptor polymorphisms independently predict response to rituximab in patients with follicular lymphoma. J Clin Oncol 2003;21:3940–7.
24. Treon SP, Hansen M, Branagan AR, Verselis S, Emmanouilides C, Kimby E, et al. Polymorphisms in FcgammaRIIIA (CD16) receptor expression are associated with clinical response to rituximab in Waldenstrom's macroglobulinemia. J Clin Oncol 2005;23:474–81.
25. Musolino A, Naldi N, Bortesi B, Pezzuolo D, Capelletti M, Missale G, et al. Immunoglobulin G fragment C receptor polymorphisms and

clinical efficacy of trastuzumab-based therapy in patients with HER-2/neu-positive metastatic breast cancer. J Clin Oncol 2008;26:1789–96.
26. Zhang W, Gordon M, Schultheis AM, Yang DY, Nagashima F, Azuma M, et al. FCGR2A and FCGR3A polymorphisms associated with clinical outcome of epidermal growth factor receptor expressing metastatic colorectal cancer patients treated with single-agent cetuximab. J Clin Oncol 2007;25:3712–8.
27. Beck A, Wagner-Rousset E, Bussat MC, Lokteff M, Klinguer-Hamour C, Haeuw JF, et al. Trends in glycosylation, glycoanalysis and glycoengineering of therapeutic antibodies and Fc-fusion proteins. Curr Pharm Biotechnol 2008;9:482–501.
28. Strohl WR. Optimization of Fc-mediated effector functions of monoclonal antibodies. Curr Opin Biotechnol 2009;20:685–91.
29. Cardarelli PM, Moldovan-Loomis MC, Preston B, Black A, Passmore D, Chen TH, et al. In vitro and in vivo characterization of MDX-1401 for therapy of malignant lymphoma. Clin Cancer Res 2009;15:3376–83.
30. Gerdes C, Friess T, Nicolini V, Freytag O, Brünker P, Späni M, et al. GA201, a novel humanized, glycoengineered EGFR antibody with enhanced ADCC and superior preclinical in vivo efficacy as single agent and in combination. In: Proceedings of the 100th Annual Meeting of the American Association for Cancer Research; 2009 April 18–22; Denver. Abstract number 5476.
31. Mossner E, Brunker P, Moser S, Puntener U, Schmidt C, Herter S, et al. Increasing the efficacy of CD20 antibody therapy through the engineering of a new type II anti-CD20 antibody with enhanced direct- and immune effector cell-mediated B-cell cytotoxicity. Blood 2010;115:4393–402.
32. Awan FT, Lapalombella R, Trotta R, Butchar JP, Yu B, Benson DM Jr, et al. CD19 targeting of chronic lymphocytic leukemia with a novel Fc-domain-engineered monoclonal antibody. Blood 2010;115:1204–13.
33. Lazar GA, Dang W, Karki S, Vafa O, Peng JS, Hyun L, et al. Engineered antibody Fc variants with enhanced effector function. Proc Natl Acad Sci USA 2006;103:4005–10.
34. Mendel DB, Laird AD, Xin X, Louie SG, Christensen JG, Li G, et al. In vivo antitumor activity of SU11248, a novel tyrosine kinase inhibitor targeting vascular endothelial growth factor and platelet-derived growth factor receptors: determination of a pharmacokinetic/pharmacodynamic relationship. Clin Cancer Res 2003;9:327–37.
35. Hu-Lowe DD, Zou HY, Grazzini ML, Hallin ME, Wickman GR, Amundson K, et al. Nonclinical antiangiogenesis and antitumor activities of axitinib (AG-013736), an oral, potent, and selective inhibitor of vascular endothelial growth factor receptor tyrosine kinases 1, 2, 3. Clin Cancer Res 2008;14:7272–83.
36. Marrone T, Hu-lowe D, Grazzini M, Yin M, Chen J, Hallin M, , et al. PF-00337210, a potent, selective and orally bioavailable small molecule inhibitor of VEGFR-2. In: Proceedings of the 98th Annual Meeting of the American Association for Cancer Research; 2007 April 14–18; Los Angeles. Abstract number 3992.
37. Mueller BM, Romerdahl CA, Trent JM, Reisfeld RA. Suppression of spontaneous melanoma metastasis in scid mice with an antibody to the epidermal growth factor receptor. Cancer Res 1991;51:2193–8.
38. Gorski KS, Waller EL, Bjornton-Severson J, Hanten JA, Riter CL, Kieper WC, et al. Distinct indirect pathways govern human NK-cell activation by TLR-7 and TLR-8 agonists. Int Immunol 2006;18:1115–26.
39. Congy-Jolivet N, Bolzec A, Ternant D, Ohresser M, Watier H, Thibault G. Fc gamma RIIIa expression is not increased on natural killer cells expressing the Fc gamma RIIIa-158V allotype. Cancer Res 2008;68:976–80.
40. Fishwild DM, O'Donnell SL, Bengoechea T, Hudson DV, Harding F, Bernhard SL, et al. High-avidity human IgG kappa monoclonal antibodies from a novel strain of minilocus transgenic mice. Nat Biotechnol 1996;14:845–51.
41. Tahtis K, Lee FT, Wheatley JM, Garin-Chesa P, Park JE, Smyth FE, et al. Expression and targeting of human fibroblast activation protein in a human skin/severe combined immunodeficient mouse breast cancer xenograft model. Mol Cancer Ther 2003;2:729–37.
42. Mancuso MR, Davis R, Norberg SM, O'Brien S, Sennino B, Nakahara T, et al. Rapid vascular regrowth in tumors after reversal of VEGF inhibition. J Clin Invest 2006;116:2610–21.
43. Leenen PJ, de Bruijn MF, Voerman JS, Campbell PA, van Ewijk W. Markers of mouse macrophage development detected by monoclonal antibodies. J Immunol Methods 1994;174:5–19.
44. Takahashi N, Haba A, Matsuno F, Seon BK. Antiangiogenic therapy of established tumors in human skin/severe combined immunodeficiency mouse chimeras by anti-endoglin (CD105) monoclonal antibodies, and synergy between anti-endoglin antibody and cyclophosphamide. Cancer Res 2001;61:7846–54.
45. Van Rooijen N, Sanders A. Liposome mediated depletion of macrophages: mechanism of action, preparation of liposomes and applications. J Immunol Methods 1994;174:83–93.
46. Horton HM, Bernett MJ, Pong E, Peipp M, Karki S, Chu SY, et al. Potent in vitro and in vivo activity of an Fc-engineered anti-CD19 monoclonal antibody against lymphoma and leukemia. Cancer Res 2008;68:8049–57.
47. Oflazoglu E, Stone IJ, Brown L, Gordon KA, van Rooijen N, Jonas M, et al. Macrophages and Fc-receptor interactions contribute to the antitumour activities of the anti-CD40 antibody SGN-40. Br J Cancer 2009;100:113–7.
48. Niwa R, Hatanaka S, Shoji-Hosaka E, Sakurada M, Kobayashi Y, Uehara A, et al. Enhancement of the antibody-dependent cellular cytotoxicity of low-fucose IgG1 Is independent of FcgammaRIIIa functional polymorphism. Clin Cancer Res 2004;10:6248–55.
49. Chahal M, Xu Y, Lesniak D, Graham K, Famulski K, Christensen JG, et al. MGMT modulates glioblastoma angiogenesis and response to the tyrosine kinase inhibitor sunitinib. Neuro Oncol 2010;12:822–33.
50. Bergers G, Hanahan D. Modes of resistance to anti-angiogenic therapy. Nat Rev Cancer 2008;8:592–603.

Cancer Research

Correction: Dual Functional Monoclonal Antibody PF-04605412 Targets Integrin α5β1 and Elicits Potent Antibody-Dependent Cellular Cytotoxicity

In this article (Cancer Res 2010;70:10243–54), which was published in the December 15, 2010 issue of *Cancer Research* (1), the top labels for the right panel of Figure 3C are incorrect. The correct labels are provided in Figure 3C below.

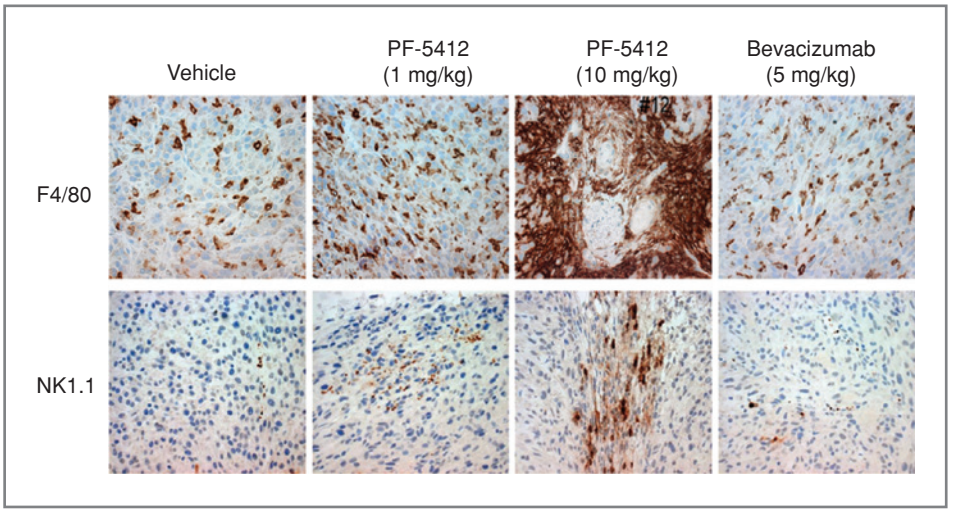

Figure 3C.

Reference

1. Li G, Zhang L, Chen E, Wang J, Jiang X, Chen JH, et al. Dual functional monoclonal antibody PF-04605412 targets integrin α5β1 and elicits potent antibody-dependent cellular cytotoxicity. Cancer Res 2010;70:10243–54.

Published onlineFirst January 18, 2011.

doi: 10.1158/0008-5472.CAN-10-4578

Dual Functional Monoclonal Antibody PF-04605412 Targets Integrin $\alpha5\beta1$ and Elicits Potent Antibody-Dependent Cellular Cytotoxicity

Gang Li, Lianglin Zhang, Enhong Chen, et al.

Cancer Res 2010;70:10243-10254.